Process and joint characterizations of laser–MIG hybrid welding of AZ31 magnesium alloy

ARTICLE *in* JOURNAL OF MATERIALS PROCESSING TECHNOLOGY · JUNE 2012

Impact Factor: 2.24 · DOI: 10.1016/j.jmatprotec.2012.01.011

5 AUTHORS, INCLUDING:

M. Gao
Huazhong University of Science and Techn…

Zemin Wang
Huazhong University of Science and Techn…

Xiangyou Li
Huazhong University of Science and Techn…

Journal of Materials Processing Technology 212 (2012) 1338–1346

Contents lists available at SciVerse ScienceDirect

Journal of Materials Processing Technology

journal homepage: www.elsevier.com/locate/jmatprotec

Process and joint characterizations of laser–MIG hybrid welding of AZ31 magnesium alloy

Ming Gao, Shuwen Mei, Zemin Wang, Xiangyou Li*, Xiaoyan Zeng

Wuhan National Laboratory for Optoelectronics, School of Optoelectronics Science and Engineering, Huazhong University of Science and Technology, Wuhan 430074, PR China

ARTICLE INFO

Article history:
Received 23 September 2011
Received in revised form 13 January 2012
Accepted 15 January 2012
Available online xxx

Keywords:
Magnesium alloy
Laser welding
Microstructure
Mechanical property

ABSTRACT

High power laser–metal inert gas (MIG) hybrid welding of AZ31 Mg alloys was studied. Microstructure and fracture surface of welded joints were observed by optical microscope and scanning electron microscope. The mechanical properties of welded joints were evaluated by tensile test. Under the optimal welding parameters, the stable process and sound joints were obtained. The tensile strength efficiency of welded joints recovered 84–98% of the substrate. It was found that the arc was compressed and stabilized by the laser beam during the hybrid welding. The compressed extent of arc column increased with laser power, and the process stability could be improved by increasing laser power and arc current or slowing welding speed. The arc stabilized mechanism in laser–MIG hybrid welding of Mg alloys was summarized in two factors. First, the laser keyhole fixes the arc root and improves the igniting ability of the arc. Second, the electromagnetic force is downward and increased by the laser–arc interaction, which prevents the overheating of the droplet and smoothes droplet transfer from the wire to the weld pool.

1. Introduction

As the lightest structural materials, magnesium (Mg) and Mg alloys have the potential to replace steel and aluminum in many fields. Because of the occurrence of weld defects such as high burning-loss, surface undercut and large porosity, they are seldom welded except for some repaired structures. Developing reliable welding techniques is thus interesting for the growing application of Mg alloys. Padmanaban et al. (2011) studied the fatigue crack growth behavior of the AZ31B Mg joints welded by tungsten inert gas (TIG), friction stir and laser beam welding. Scintilla et al. (2010) investigated laser beam welding of AZ31 Mg alloys and obtained good welds. Liu et al. (2004, 2008) developed low power laser–TIG hybrid welding to join Mg alloys, which indicated laser–arc hybrid welding would be an effective method to suppress the metallurgical defects and increase the mechanical properties of Mg joints.

High power laser–metal inert gas (MIG) hybrid welding has been considered to be the most promising and popular method because of its deep weld penetration, high welding efficiency, good joining strength and strong ability to reduce weld deficiencies. Unfortunately, there were few reports on laser–MIG hybrid welding of Mg alloys because of their special physical characteristics. The vaporization temperature of Mg (about 1373 K) is only half of aluminum and its vaporization pressure in the temperature interval during MIG welding is 10^3 up to 10^4 higher than that of aluminum, which leads to the droplet be overheated easily during MIG welding of Mg alloys because the possible temperature interval on the droplet is very small. The overheated droplet explodes sensitively due to the high vaporization pressure of Mg, resulting in a great spatter and a very unstable process without a secure drop detachment. Thus, MIG welding of Mg alloys is very difficult. Only two special MIG welding methods obtained sound Mg joints: the triggered short-circuiting arc welding developed by Wohlfahrt et al. (2003) and the AC-MIG welding presented by Song et al. (2010). This situation hampered the development of laser–MIG hybrid welding of Mg alloys.

As the unstable arc could be stabilized by laser–arc interaction during the hybrid welding, Gao et al. (2009a) had reported a preliminary result to obtain one accepted joint by laser–MIG hybrid welding of AZ31 Mg alloy. It suggested the unstable problem in the laser–MIG hybrid welding of Mg alloys might be overcome by optimizing the interaction of two heat sources. However, there lack comprehensive investigations into effects of welding parameters on process characterization and joint performance. This article aims to deepen the understanding of laser–MIG hybrid welding of Mg alloys by presenting more experiment results.

2. Experimental work

A 5 kW Rofin-Sinar TR050 CO_2 laser and a Panasonic pulse MIG welder were used. The laser beam was focused by a copper mirror with a focal length of 286 mm to get a focal diameter of 0.6 mm. The base materials (BM) were commercial AZ31 and AZ31B wrought Mg

* Corresponding author. Tel.: +86 27 87792404; fax: +86 27 87541423.
E-mail address: xyli@mail.hust.edu.cn (X. Li).

0924-0136/$ – see front matter
doi:10.1016/j.jmatprotec.2012.01.011

Table 1
Chemical composition and mechanical properties of base materials and filler wire.

Materials	Chemical composition (wt%)								Mechanical properties	
	Al	Zn	Mn	Si	Fe	Cu	Ni	Mg	UTS (MPa)	EL (%)
BM AZ31B	2.5–3.5	0.5–1.5	0.2–0.6	≤0.1	≤0.005	≤0.05	≤0.005	Balance	250	15
BM AZ31	3.5–4.5	0.8–1.4	0.3–0.6	≤0.1	≤0.005	≤0.05	≤0.005	Balance	268	18
Wire AZ31B	2.5–3.5	0.5–1.2	0.2–0.5	≤0.1	≤0.005	≤0.05	≤0.005	Balance	–	–

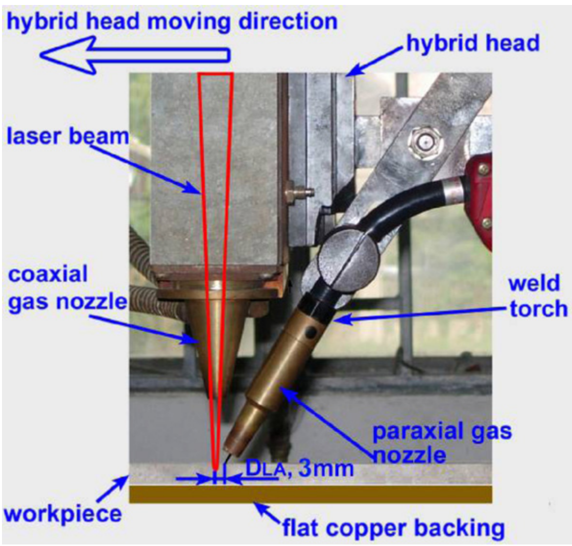

Fig. 1. Experimental set-up of laser–MIG hybrid welding.

alloys and the filler wire was AZ31 Mg alloy with the diameter of 1.6 mm. Table 1 shows the chemical compositions and mechanical properties of base materials and filler wire. The thickness of the AZ31 plate was 10 mm, while that of the AZ31B plate was 5 mm. Before welding, they were milled to be 100 mm × 100 mm and then cleaned by acetone.

Fig. 1 shows the arrangement of heat sources, which has been optimized in previous studies (Gao et al., 2009a,b). During welding, a flat copper backing was used to force the formation of weld root. The paraxial weld torch was 55° angle to the surface of workpiece by using a He–Ar (3:2) mixed gas flux of 25 l/min. A coaxial gas nozzle was employed to protect the focal mirror by using a pure argon gas flux of 7.5 l/min. The distance between laser beam and wire tip (D_{LA}) was 3 mm, and the laser defocused distance was −1 mm.

The study on the process characterization was carried out in the configuration of bead-on-plate, while that on the joint characterization was carried out in butt configuration. Table 2 shows the welding parameter range used for process characterization. Table 3 shows the welding parameters selected for microstructure analysis and tensile test. Table 4 shows the detailed arc parameters corresponding to each current. Where P denotes the laser power, I denotes the arc current, U denotes the arc voltage, v denotes the welding speed, Q denotes the heat input, r denotes the wire feed rate and f denotes pulse frequency of the arc. The heat ratio of arc to laser was defined as HRAL and presented as follows:

$$\mathrm{HRAL} = \frac{U \times I}{P} \tag{1}$$

Table 2
Parameter range used for process characterization.

Welding parameter	Range
Laser power, P (kW)	1.5–4.5
Arc current, I (A)	60–210
Welding speed, v (m/min)	1.0–2.0

Table 3
Welding parameters selected for microstructure analysis and tensile samples.

No.	BM	Welding parameter			HRAL	Q (J/mm)
		P (kW)	I (A)	v (m/min)		
Hy1	AZ31	2.5	120	0.5	1.06	616.8
Hy2	AZ31	3.5	120	0.5	0.75	736.8
Hy3	AZ31	3.5	120	1.0	0.75	368.4
Hy4	AZ31	3.5	120	1.2	0.75	307.0
Hy5	AZ31	4.5	120	2.0	0.59	214.2
Hy6	AZ31B	3.0	90	2.4	0.60	120.0
Hy7	AZ31B	3.0	150	2.4	1.20	165.0
Hy8	AZ31B	3.0	210	2.4	2.10	232.5
Hy9	AZ31B	3.0	150	1.2	1.20	330.0
Hy10	AZ31B	2.0	150	1.2	1.80	280.0
Hy11	AZ31B	4.0	120	3.2	0.66	124.5

Table 4
Detailed parameters corresponding to each arc current, all used arcs have the same base and peak current of 50 A and 380 A, respectively.

	I (A)				
	90	120	150	180	210
U (V)	20	22	24	27	30
f (Hz)	54	72	90	108	126
r (m/min)	3.2	4.4	5.4	6.6	7.8

After welding, the metallurgical samples were prepared by standard metallographic procedures and etched by a solution containing 4.2 g picric acid, 10 ml acetic acid, 10 ml water and 100 ml ethanol with an etching time of about 20 s. The microstructure and fracture surface were analyzed by optical and scanning electron microscopy (SEM), respectively. The tensile samples were prepared according to the drawing shown in Fig. 2 and tested at room temperature. The result was the average value of three samples.

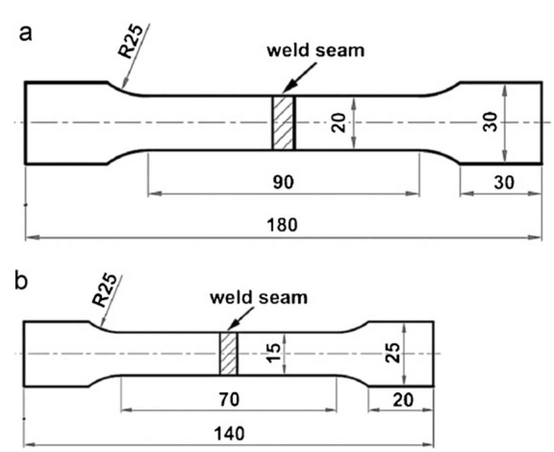

Fig. 2. Drawings of tensile specimens, (a) 10 mm AZ31 and (b) 5 mm AZ31B.

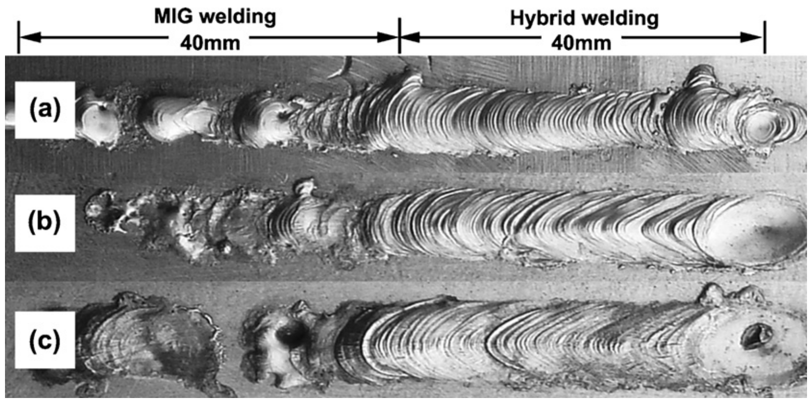

Fig. 3. Effects of arc current on bead surface morphologies (AZ31 alloy with the thickness of 10 mm). The arc current is (a) $I = 150$ A, (b) $I = 180$ A and (c) $I = 210$ A, while in hybrid welding the laser power keeps 3.0 kW. The welding speed is 1.0 m/min for all specimens.

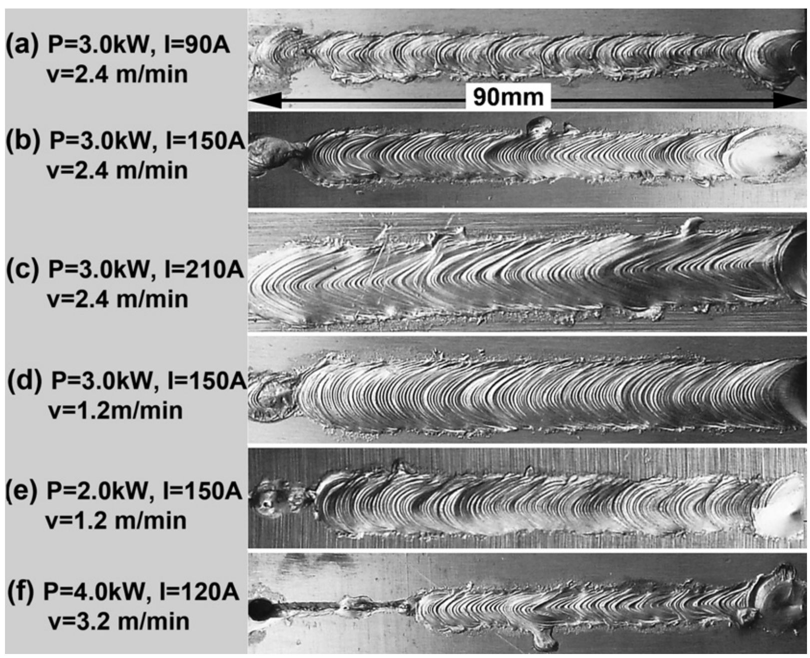

Fig. 4. Surface morphologies of hybrid welds in butt configuration (AZ31B alloy with the thickness of 5 mm).

3. Results

3.1. Process characterization

Since the bead surface is an important reflection of the process stability and can be observed by naked eyes directly, it was used to evaluate the process characterization. Regular and continuous surface denotes a stable process, while irregular and discontinuous surface indicates an unstable process. To discover the laser–arc interaction during hybrid welding, the shapes of laser induced plasma and arc column were recorded by a CCD camera. As shown in Fig. 3, despite the fact that all possible welding parameters were used, pure MIG welding obtains discontinuous and irregular welds, indicating an unstable process. However, the sound weld and stable process are obtained in the hybrid welding under appropriate welding parameters. If the arc current is too small or the welding speed is too fast, as shown in Fig. 4a andf, hybrid welding shows some undesired surface morphologies with the defects of overlap, undercut and discontinuity. Increasing arc current and laser power, or decreasing welding speed could help stabilize the hybrid welding and improve the quality of bead surface, as shown in Fig. 4b–d.

In Fig. 5, the arc column is compressed by the laser beam during hybrid welding compared to the shape in pure MIG welding. When the laser power keeps constant, the compressed extent of arc column reduces with increasing arc current because the self-ionization or self-stability of the arc column enhances gradually with increasing arc current. The similar phenomenon was also observed by Chen et al. (2006). As shown in Fig. 6, the higher the laser power is, the bigger the compressed extent of the arc column is. Based on above descriptions in the process stability, a strong link would be exist between the plasma shape and the process stability during the hybrid welding of Mg alloy, which will be discussed in Section 4.1.

3.2. Effects of welding parameters on bead shape

As shown in Fig. 7, the penetration depth of hybrid welds increases with both the laser power and the arc current, and the increase caused by laser power is more obvious. The increment in penetration depth caused by laser power is 2–3 mm per kilowatt, while that caused by arc power is about 0.5 mm per kilowatt. In addition, the penetration depth of hybrid weld is bigger than that of pure laser weld as the laser power and

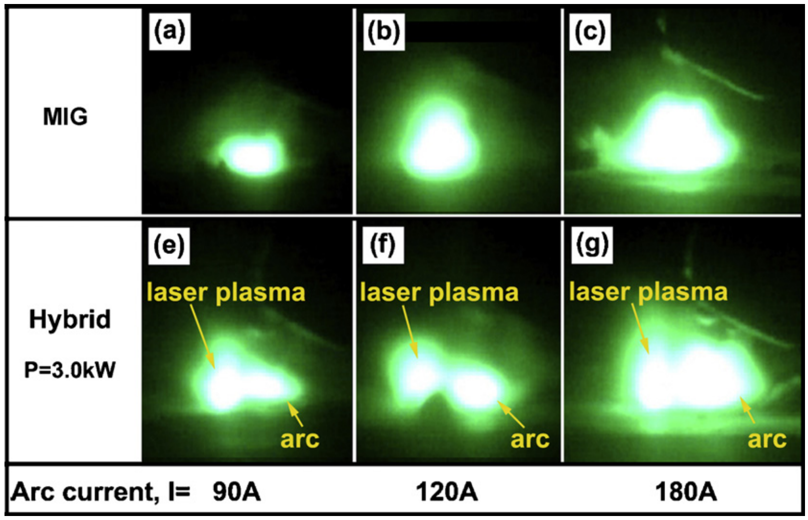

Fig. 5. Plasma shapes in pure MIG welding and hybrid welding at $v = 1.0$ m/min (top single MIG welding to bottom hybrid welding), the base material is AZ31 alloy with the thickness of 10 mm.

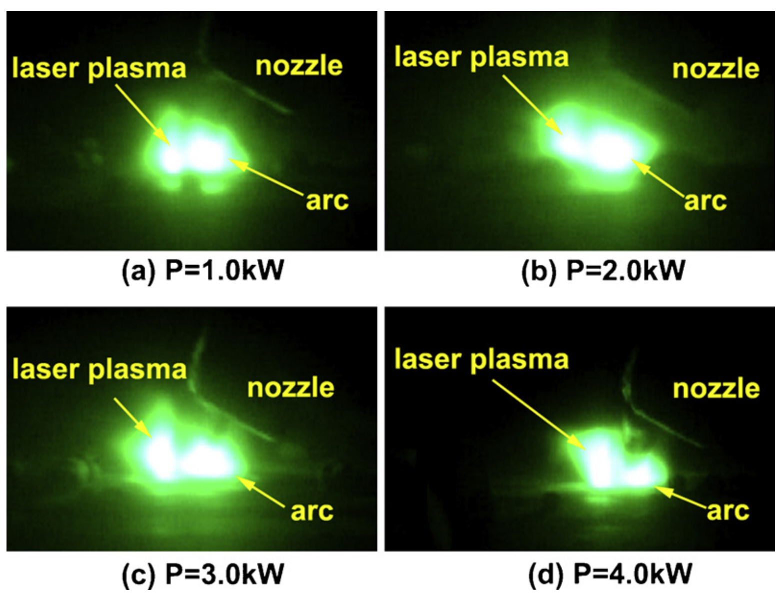

Fig. 6. Effects of laser power on the compression of arc column in hybrid welding with $I = 150$ A and $v = 1.0$ m/min, the base material is AZ31 alloy with the thickness of 10 mm.

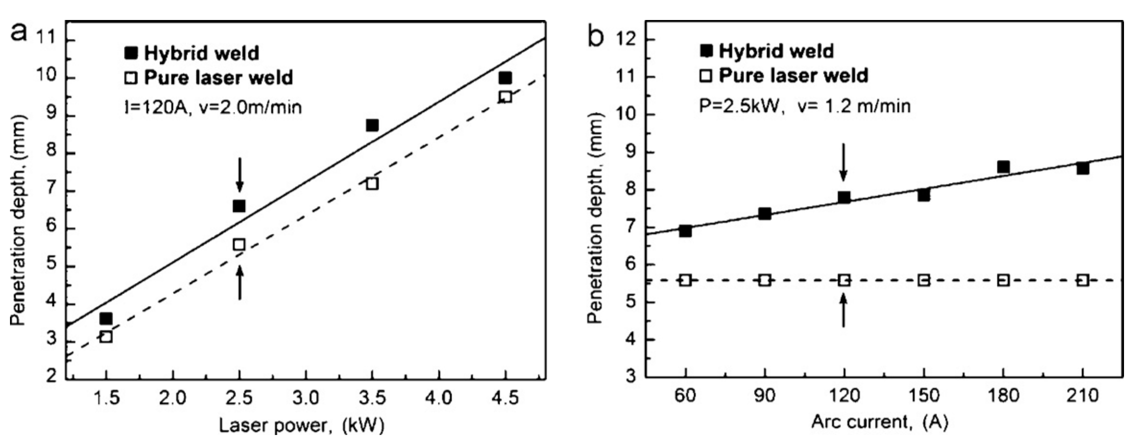

Fig. 7. Effects of laser power (a) and arc current (b) on penetration depth of AZ31 hybrid weld, the solid and dash lines are the penetration depth of hybrid weld and pure laser weld respectively, and the arrowed points are the welds for comparison.

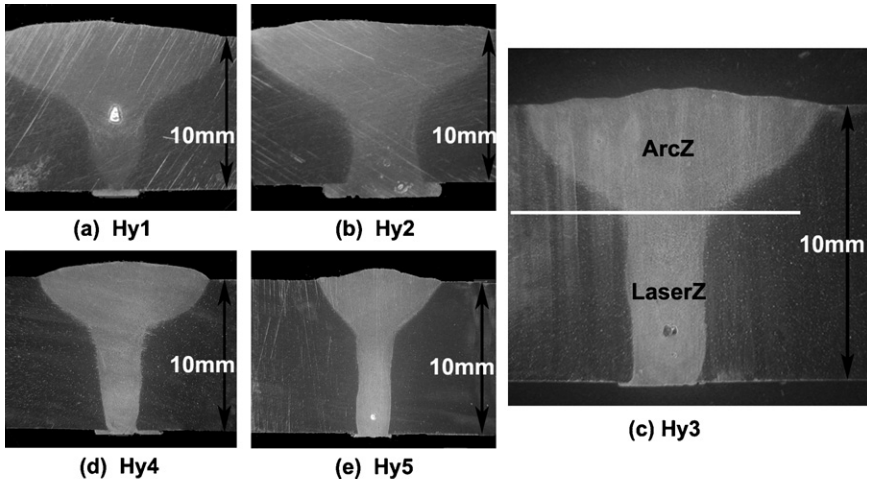

Fig. 8. Effects of welding parameters on transverse morphologies of hybrid welds whose welding parameters are shown in Table 3.

welding speed keep the same, and the increment in penetration depth of hybrid weld to laser weld varies with the welding speed. For example, when the arc current is 120 A and laser power is 2.5 kW, the penetration depth increment of hybrid weld to laser weld is only 1 mm (~18% of laser weld) at the welding speed of 2.0 m/min, as arrowed in Fig. 7a, whereas it reaches 2.1 mm (~40% of laser weld) at the welding speed of 1.2 m/min, as arrowed in Fig. 7b.

In Fig. 8, the hybrid welds have typical 'wine-cup' shapes. The wide upper zone has the characteristic of arc welds, while the narrow lower zone has the characteristic of laser welds. In brief, as shown in Fig. 8c, the upper and lower zones are defined as ArcZ and LaserZ, respectively. Fig. 8 shows the weld shape varies with the welding parameters. In Fig. 8d and e, the width of ArcZ decreases by 1.4 times as the welding speed reduces from 2.0 m/min (Hy5) to 1.2 m/min (Hy4). In Fig. 8a and b, the width of LaserZ increases by 1.5 times as the laser power increases from 2.5 kW (Hy1) to 3.5 kW (Hy2). These changes indicate the width of ArcZ decreases with increasing welding speed due to the increasing heat input, while the width of LaserZ depends on the laser power.

3.3. Microstructure

Some typical welds in Table 3 are selected for the microstructure analysis. As shown in Fig. 9, the microstructure of BM is massive α-Mg grains with the average size of 25 μm. A partial melted zone (PMZ) is observed near the fusion zone (FZ), and the PMZ width of LaserZ and ArcZ varies with the laser power and the arc current. In Fig. 9a and c, the PMZ in ArcZ of joint Hy1 and Hy4 almost has the same width when the arc current keeps constant, though the laser power increases from 2.5 kW to 4.5 kW. However, as shown in Fig. 9b and d, the PMZ width in LaserZ of joint Hy4 is bigger than that of joint Hy1 due to the increase of laser power.

Fig. 10 shows the microstructure of FZ consists of dendrites. As analyzed by Chowdhury et al. (2011) and Gao et al. (2011), the bright arms are α-Mg and a small quantity of β-$Mg_{17}(Al,Zn)_{12}$

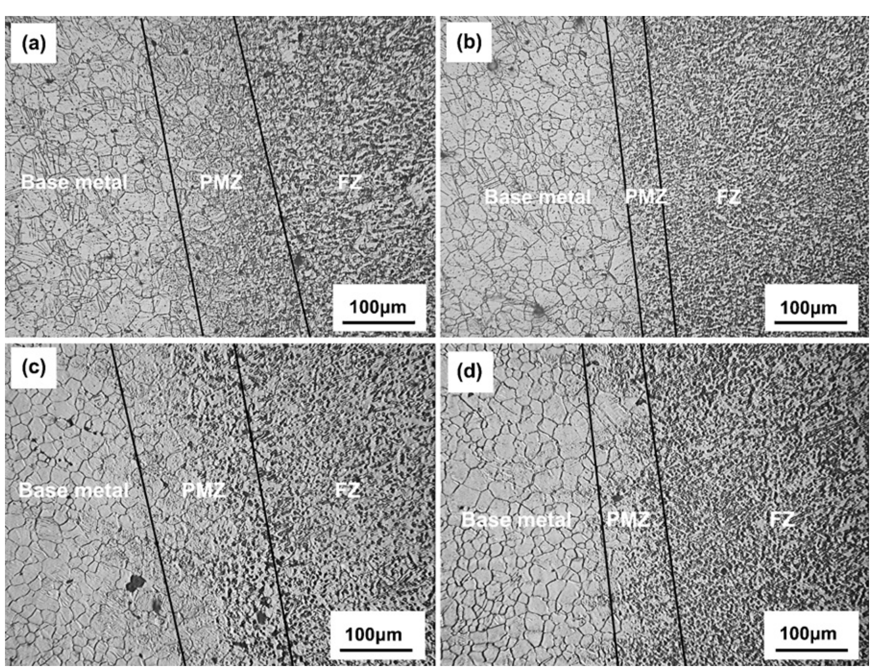

Fig. 9. Overview of the microstructure for typical hybrid welds of AZ31 alloy, (a) ArcZ of joint Hy1, (b) LaserZ of joint Hy1, (c) ArcZ of joint Hy4 and (d) LaserZ of joint Hy4.

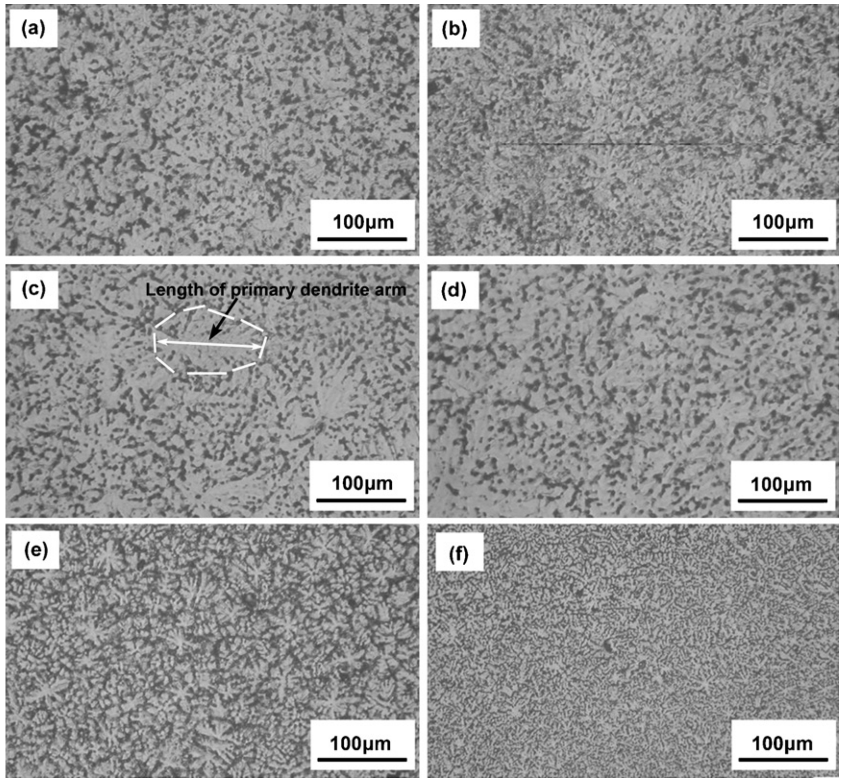

Fig. 10. Difference of the microstructure between ArcZ and LaserZ, (a) ArcZ of Hy1, (b) LaserZ of Hy1; (c) ArcZ of Hy2, (d) LaserZ of Hy2, (e) ArcZ of Hy3 and (f) LaserZ of Hy3.

precipitates in the α-Mg or between the arms during the solidification. Although scattering exists, the length of the primary dendrite arm shown in Fig. 10c was measured and averaged to evaluate the effects of the welding parameters on the size of the solidification structures. The average lengths of primary dendrite arm in ArcZ for the joint Hy1 and Hy3 are 80 μm and 40 μm as shown in Fig. 10a and e, while those in LaserZ are 50 μm and 10 μm as shown in Fig. 10b and f. That is, the length ratio of ArcZ to LaserZ is 1.6 and 3 for joint Hy1 and Hy3, respectively. It indicates the difference in the size of solidification structures between the ArcZ and the LaserZ reduces with increasing HRAL when the arc current keeps the same. Gao et al. (2008) found that increasing HRAL means more arc heat is transferred into the lower part of molten pool to homogenize the heat distribution in total molten pool due to the increasing arc pressure, and accordingly reduces the difference in the solidification structures between the ArcZ and the LaserZ. Besides, as shown in Fig. 10d and f, the decrease of welding speed coarsens the solidification structure obviously because of the increase of heat input.

3.4. Tensile strength

The tensile properties are listed in Table 5. To evaluate the tensile properties of welded joints, the ultimate tensile strength (UTS) and elongation (EL) efficiency were calculated by following formulas:

$$\text{UTS efficiency} = \frac{\text{Joint UTS}}{\text{BM UTS}} \times 100\% \tag{2}$$

$$\text{EL efficiency} = \frac{\text{Joint EL}}{\text{BM EL}} \times 100\% \tag{3}$$

The UTS efficiency is in the range of 84–98%, and the EL efficiency of AZ31 and AZ31B alloy is in the range of 39–78% and 27–60%, respectively. Most of the joints fracture in the FZ, but a few joints with higher UTS efficiency (about 95%) fracture in the heat affected zone (HAZ). These results show laser–MIG hybrid welding is an effective joining method for Mg alloy and has the ability to obtain sound joints with good mechanical properties.

3.5. Fracture behavior

In Fig. 11, many pores appear on the fracture surface of the welded joints cracked in the FZ. The porosity of the welded joints was measured by an image program (Photoshop CS4) and calculated by the following formula:

$$\text{Porosity} = \frac{A_p}{A_0} \times 100\% \tag{4}$$

where A_p is the area of pores on the fracture surface, A_0 is the area of whole fracture surface. It can be found that the porosity reduces with increasing arc current. As the arc current increases from 90 A to 150 A and 210 A, the porosity reduces from 11% to 4% and 3% in sequence. In addition, the fracture surface of the joint Hy9 is free of pores because it fractures in the HAZ.

As shown in Fig. 12a andb, the fracture surfaces are mainly characterized by dimple patterns but with remarkably tearing ridges showing the brittle features. The dimples result from the weld matrix, soft α-Mg with good ductility, whereas the tearing ridges are caused by the pores and brittle precipitated phase at grain boundaries. In Fig. 12c, some plastic oxide inclusions are found on the fracture surface. It indicates the oxide inclusion in the FZ is one of the reasons to decrease the joining strength of hybrid welds. Besides, some smooth depressions with slipping strips are also observed on the fracture surface, as pointed by the rectangle outlined area in Fig. 12b. The details in Fig. 12d suggest it is not truly smooth, but exhibits a uniform array of fine slide striations and a few of minute dimples.

Table 5
Tensile results and fracture location (Hy1–Hy5: AZ31, Hy6–Hy10: AZ31B).

No.	UTS (MPa)				UTS efficiency (%)	EL (%)				EL efficiency (%)	Fracture location
	1	2	3	Average		1	2	3	Average		
Hy1	233	238	237	236	88	7	7	7	7	39	FZ
Hy2	222	228	225	225	84	7	8	9	8	44	FZ
Hy3	256	248	255	253	94	12	11	11	11	61	HAZ
Hy4	265	259	262	262	98	13	14	14	14	78	HAZ
Hy5	251	255	259	255	95	10	10	9	10	56	FZ
Hy6	198	218	210	212	85	3	5	4	4	27	FZ
Hy7	215	220	219	218	87	5	5	4	5	33	FZ
Hy8	232	230	222	228	91	6	6	5	6	40	FZ
Hy9	242	235	243	240	96	9	9	10	9	60	HAZ
Hy10	217	213	218	216	86	6	5	5	5	33	FZ
Hy11	215	223	222	220	88	5	5	4	5	33	FZ

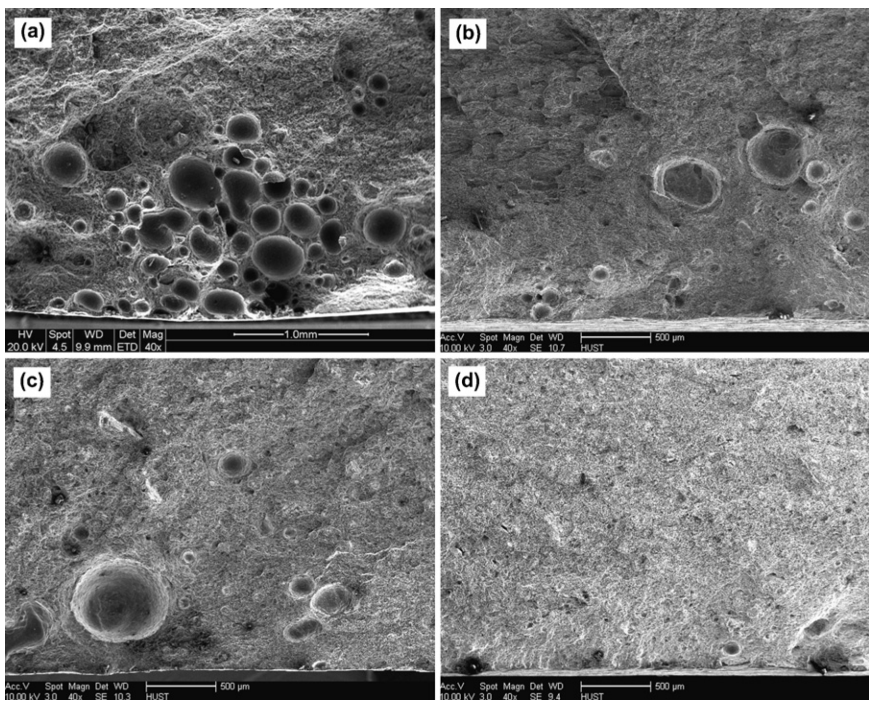

Fig. 11. Macro morphologies of fracture surface, (a) Hy6, (b) Hy7, (c) Hy8 and (d) Hy9.

4. Discussion

4.1. Arc stabilized mechanism

According to the reported theory in laser–arc hybrid welding and the physical characterization of pure MIG welding of Mg alloy, the arc stabilized mechanism in current study is described as the following two factors.

First, the truth that laser keyhole or laser induced plasma plume fixes the arc root during the hybrid welding to improve the igniting ability of the arc. According to the principle of minimum voltage, the arc prefers to pass through the channel with higher conductivity. Because the laser keyhole consists of large amount of high temperature electrons and metallic ions, its conductivity is far higher than that of cold substrate. The arc is then easily fixed and led by laser keyhole rather than wanders as it is usually in pure MIG welding. In the study of laser–MIG hybrid welding carried out by Sugino et al. (2004), an obvious electronic channel was observed between the laser plasma and the arc column, as shown in Fig. 13, indicating obvious leading effect of laser beam on arc root. Based on this laser leading effect, the arc can burn continually or be ignited again rapidly during the hybrid welding after extinguishing temporarily by the explosion of the overheated droplet. Accordingly, a relative stable process is achieved in the hybrid welding.

Second, the laser–arc interaction prevents the overheating of the droplet and smoothes its transfer from the wire tip to the weld pool. Before the discussion, we need refer to the transfer mechanism of the droplet in pure arc welding. Nemchinsky (1996) reported electromagnetic force plays a decisive role in the droplet transfer during the arc welding. In the arc, the magnitude and direction of electromagnetic force depends on the current distribution and the discharge direction. Provided that the droplet has a large anode spot as shown in Fig. 14a, the current flow diverges. The electromagnetic force applies in the same direction as the arc discharge, and detaches the droplet from the wire tip. In contrast, the current flow converges when the droplet has a small anode spot as shown in Fig. 14b. The electromagnetic force is upward and attaches the droplet on the wire tip. Based on this theory, the other arc stabilized mechanism during hybrid welding of Mg alloy is explained as follows.

For the pure MIG welding of Mg alloy, the arc root is almost wandering throughout the welding process owing to the frequent explosion of the overheated droplet. It causes the anode spot on the droplet is erratic and small as shown in Fig. 14b. The

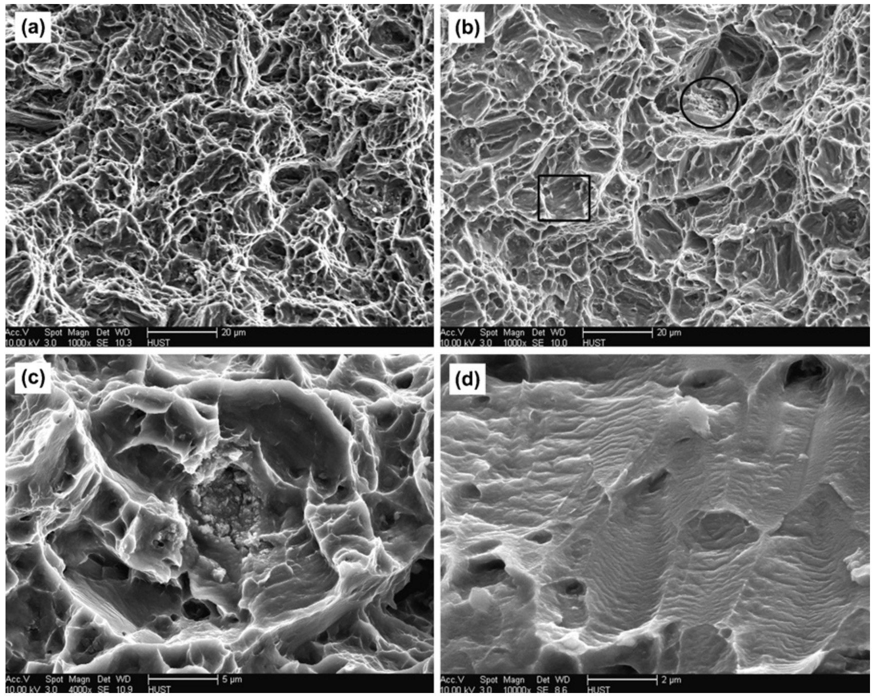

Fig. 12. SEM morphologies of fracture surfaces at high magnifications, (a) Hy6 at 1000×, (b) Hy8 at 1000×, (c) details of circle-outlined area in (b) at 4000× and (d) details of rectangle-outlined area in (b) at 10,000×.

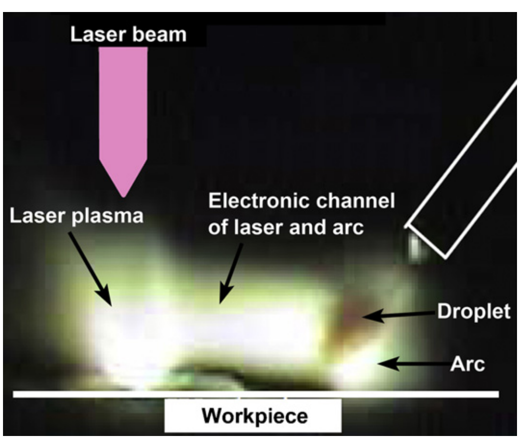

Fig. 13. Experimental observation of the interaction between laser induced plasma and arc column in laser–MIG hybrid welding carried out by Sugino et al. (2004).

electromagnetic force is then upward to attach the droplet on the wire tip. It increases the overheated extent at the neck of the droplet, and further increases the explosion sensitivity of the droplet. As a result, the stable process is hard to be obtained during pure MIG welding of Mg alloy.

During the hybrid welding, the arc burns steadily because the arc root is fixed and stabilized by the laser keyhole as mentioned above. A big anode spot on the droplet is then obtained as shown in Fig. 14a, and the electromagnetic force is downward to detach the droplet to weld pool. Meanwhile, as reported by Bagger and Olsen (2005), the charged particles in laser induced plasma tends to migrate to arc column because the density and temperature of the charged particles in laser induced plasma is far higher than that in arc column. This migration increases the ionization degree and the temperature in the arc column, and thus compresses the arc column. The shrinkage of arc column increases the current density in it. Because the magnitude of electromagnetic force is proportional to the square of arc current as reported by Robert and Messler (2004), the magnitude of electromagnetic force during hybrid welding also

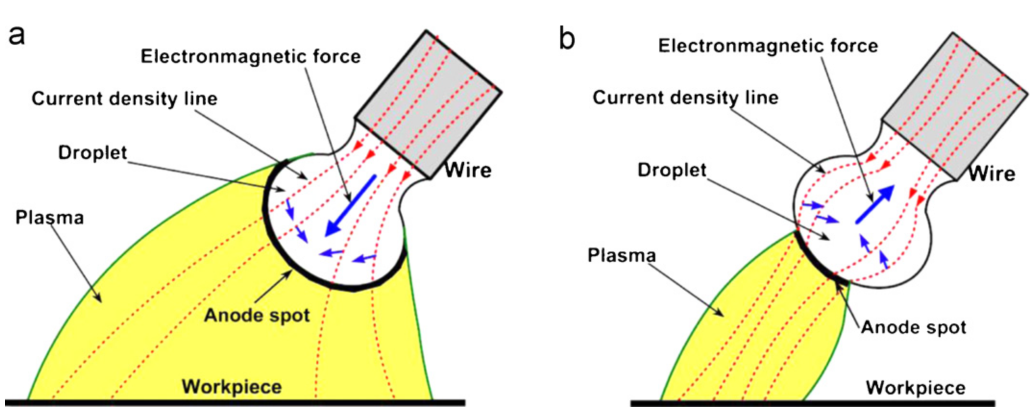

Fig. 14. Electromagnetic force and current density lines inside the droplet and adjacent plasma. (a) Electromagnetic force detaches the droplet with diverging current lines. (b) Electromagnetic force attaches the droplet with converging current lines.

increases compared with pure MIG welding. Consequently, a downward and increased electromagnetic force could be obtained in hybrid welding, which is favorable for smoothing the transfer of the droplet and improving the stability of laser–MIG hybrid welding of Mg alloy.

4.2. Relationship between welding parameter and joint performance

According to above experimental observations we found that the UTS efficiency and fracture mode of welded joints depend on the porosity and solidification structures in the FZ. Since both the porosity and solidification structures are dominated by welding parameters, the relationship between the welding parameters and the joint performances is worth discussing.

Zhou et al. (2003) demonstrated the arc pressure and surface tension induce a vortex in the molten pool during the hybrid welding. Assisted by the flow of this vortex, the bubbles coming from the growth of original micro-void in base material (Yu et al., 2009) and the collapse of unstable laser keyhole (Cao et al., 2006) can escape from the molten pool to the air. Because higher HRAL is corresponding to larger arc current with bigger arc pressure, increasing HRAL accelerates the flow speed of the vortex by increasing arc pressure, and meanwhile it both enlarges the volume of ArcZ and prolongs the solidification time by increasing arc heat. The bubbles in the molten pool with higher HRAL then have faster speed, bigger area and longer time to escape to the air, resulting in the reduction of the porosity. When the HRAL is constant, slowing welding speed has the same impacts because it increases the total heat input and prolongs the acting time of arc pressure per length. If the welding speed is too slow, the solidification structures in the FZ will become too coarse due to excessive heat input. These discussions indicate the match of higher HRAL and moderate welding speed is necessary to obtain a sound joint with few pores and fine solidification structures.

The other notable thing is that a few joints with higher UTS efficiency (about 95%) fracture in the HAZ. Table 5 shows these joints all employ a relatively slow welding speed (~1.0 m/min), resulting a relatively large heat input. It means the liquation and over-aging of the HAZ may occur and make the HAZ be the softest area of welded joint. This phenomenon has been proved by the microhardness distribution of joint Hy4 by Gao et al. (2009a). As reported by Ren et al. (2007), the softest zone is usually the weakest part of welded joints for the wrought alloys so that the joints prefer to initially fracture in the HAZ when the weld porosity and coarse solidification structure are avoided.

5. Conclusions

(1) Stable process and sound joints were obtained in laser–MIG hybrid welding of AZ31 Mg alloys. It was found that the arc column was compressed by the laser beam during the welding. The penetration depth of hybrid welds increases with both the laser power and the arc current, and the increase caused by laser power is more obvious. The increment in penetration depth caused by laser power is 2–3 mm per kilowatt, while that caused by arc power is about 0.5 mm per kilowatt.
(2) The difference in the size of the solidification structures is found between the ArcZ and the LaserZ, which can be reduced by increasing the HRAL or decreasing the welding speed.
(3) The UTS efficiency of hybrid welds is in the range of 84–98%. Under the optimized welding parameters, the UTS efficiencies of the welded joints are about 95% due to the low porosity and fine solidification structures in the FZ.
(4) The arc stabilized mechanism in the laser–MIG hybrid welding of Mg alloys is concluded as two factors. First, the laser keyhole fixes the arc root and improves the igniting ability of the arc. Second, the electromagnetic force is downward and increased by the laser–arc interaction, which prevents the overheating of the droplet and smoothes droplet transfer from the wire to the weld pool.

Acknowledgments

The authors gratefully acknowledge the supports of National 863 High Technology Research and Development Program of China with grant no. 2008AA030116 and Ph.D. Program Foundation of Ministry of Education of China with grant no. 200804871013.

References

Bagger, C., Olsen, F.O., 2005. Review of laser hybrid welding. J. Laser Appl. 17, 2–14.
Cao, X., Jahazi, M., Immarigeon, J.P., 2006. A review of laser welding techniques for magnesium alloys. J. Mater. Process. Technol. 171, 188–204.
Chen, Y.B., Lei, Z.L., Li, L.Q., Wu, L., 2006. Experimental study on welding characteristics of CO_2 laser TIG hybrid welding process. Sci. Technol. Weld. Join. 11, 403–411.
Chowdhury, S.M., Chen, D.L., Bhole, S.D., Powidajko, E., 2011. Microstructure and mechanical properties of fiber-laser-welded and diode-laser-welded AZ31 magnesium alloy. Metall. Mater. Trans. A 42, 1974–1989.
Gao, M., Zeng, X.Y., Hu, Q.W., 2008. Weld shape and microstructure of laser–arc hybrid welding. Sci. Technol. Weld. Join. 13, 106–113.
Gao, M., Zeng, X.Y., Tan, B., Feng, J.C., 2009a. Study of laser MIG hybrid welded AZ31 magnesium alloy. Sci. Technol. Weld. Join. 14, 274–281.
Gao, M., Tan, B., Feng, J.C., 2009b. Effects of welding parameters on weld shape of laser–MIG hybrid welding of AZ31 magnesium alloy. Chin. J. Nonferrous Met. 19, 222–227 (in Chinese).
Gao, M., Wang, Z.M., Yan, J., Zeng, X.Y., 2011. Dissimilar Ti/Mg alloy butt welding by fibre laser with Mg filler wire – preliminary study. Sci. Technol. Weld. Join. 16, 488–496.
Liu, L.M., Wang, J.F., Song, G., 2004. Hybrid laser–TIG welding, laser beam welding and gas tungsten arc welding of AZ31B magnesium alloy. Mater. Sci. Eng. A 381, 129–133.
Liu, L.M., Song, G., Zhu, M.L., 2008. Low-power laser–arc hybrid welding behavior in AZ-based Mg alloys. Metall. Mater. Trans. A 39A, 1702–1711.
Nemchinsky, V.A., 1996. The effect of the type of plasma gas on current constriction at the molten tip of an arc electrode. J. Phys. D: Appl. Phys. 29, 1202–1208.
Padmanaban, G., Balasubramanian, V., Madhusudhan Reddy, G., 2011. Fatigue crack growth behaviour of pulsed current gas tungsten arc, friction stir and laser beam welded AZ31B magnesium alloy joints. J. Mater. Process. Technol. 211, 1224–1233.
Ren, S.R., Ma, Z.Y., Chen, L.Q., 2007. Effect of welding parameters on tensile properties and fracture behavior of friction stir welded Al–Mg–Si alloy. Scripta Mater. 56, 69–72.
Robert, W., Messler Jr., 2004. Principles of Welding, 2nd ed. Willey-VCH, New York, pp. 216–269.
Scintilla, L.D., Tricarico, L., Brandizzi, M., Satriano, A.A., 2010. Nd:YAG laser weldability and mechanical properties of AZ31 magnesium alloy butt joints. J. Mater. Process. Technol. 210, 2206–2214.
Song, G., Wang, P., Liu, L.M., 2010. Study on ac-PMIG welding of AZ31B magnesium alloy. Sci. Technol. Weld. Join. 15, 219–225.
Sugino, T., Tsukamo, S., Nakamura, T., Arakane, G., 2004. Fundamental study on welding phenomena in pulsed laser–GMA hybrid welding. In: Proceeding of 23rd ICALEO, Miami, USA, pp. 108–116 (Paper 302).
Wohlfahrt, H., Rethmeier, M., Bouaifi, H.B., Schulz, M., 2003. Metal-inert gas welding of magnesium alloy. Weld. Cutt. 55, 80–84.
Yu, L., Nakata, K., Liao, J., 2009. Weld porosity in fibre laser weld of thixomolded heat resistant Mg alloys. Sci. Technol. Weld. Join. 14, 554–558.
Zhou, J., Zhang, W.H., Tsai, H.L., 2003. Modeling the transport phenomena during hybrid laser–MIG welding process. In: Proceeding of IMECE'03, Washington, DC, USA, pp. 1–8 (paper IMECE2003-41703).